JOURNAL OF STRUCTURAL BIOLOGY **120,** 11–21 (1997)
ARTICLE NO. SB973902

IRIS Explorer Software for Radial-Depth Cueing Reovirus Particles and Other Macromolecular Structures Determined by Cryoelectron Microscopy and Image Reconstruction

Stephan M. Spencer[1]

Institute for Molecular Virology and Department of Biochemistry, University of Wisconsin-Madison, Madison, Wisconsin 53706

Jean-Yves Sgro

Institute for Molecular Virology, University of Wisconsin-Madison, Madison, Wisconsin 53706

Kelly A. Dryden[2]

Department of Microbiology and Molecular Genetics, Harvard Medical School, Boston, Massachusetts 02115

Timothy S. Baker

Department of Biological Sciences, Purdue University, West Lafayette, Indiana 47907

and

Max L. Nibert[3]

Institute for Molecular Virology and Department of Biochemistry, University of Wisconsin-Madison, Madison, Wisconsin 53706

Structures of biological macromolecules determined by transmission cryoelectron microscopy (cryo-TEM) and three-dimensional image reconstruction are often displayed as surface-shaded representations with depth cueing along the viewed direction (Z cueing). Depth cueing to indicate distance from the center of virus particles (radial-depth cueing, or R cueing) has also been used. We have found that a style of R cueing in which color is applied in smooth or discontinuous gradients using the IRIS Explorer software is an informative technique for displaying the structures of virus particles solved by cryo-TEM and image reconstruction. To develop and test these methods, we used existing cryo-TEM reconstructions of mammalian reovirus particles. The newly applied visualization techniques allowed us to discern several new structural features, including sites in the inner capsid through which the viral mRNAs may be extruded after they are synthesized by the reovirus transcriptase complexes. To demonstrate the broad utility of the methods, we also applied them to cryo-TEM reconstructions of human rhinovirus, native and swollen forms of cowpea chlorotic mottle virus, truncated core of pyruvate dehydrogenase complex from *Saccharomyces cerevisiae,* and flagellar filament of *Salmonella typhimurium*. We conclude that R cueing with color gradients is a useful tool for displaying virus particles and other macromolecules analyzed by cryo-TEM and image reconstruction.

INTRODUCTION

Transmission cryoelectron microscopy (cryo-TEM)[4] combined with three-dimensional (3-D) image reconstruction provides a complement to X-ray crystallog-

[1] Present address: Internet Concepts, 931 East Main St., Madison, WI 53703.

[2] Present address: School of Biological Sciences, University of Auckland, Private Bag 92019, Auckland, New Zealand.

[3] To whom correspondence and reprint requests should be addressed at Institute for Molecular Virology, University of Wisconsin-Madison, 1525 Linden Drive, Madison, WI 53706. Fax: (608) 262-7414. E-mail: MLNIBERT@FACSTAFF.WISC.EDU.

[4] Abbreviations used: 3-D, three-dimensional; CCMV, cowpea chlorotic mottle virus; cryo-TEM, transmission cryoelectron microscopy; HRV14, human rhinovirus, serotype 14; ISVP, infectious subvirion particle; PDH, pyruvate dehydrogenase; R-cued, radially depth-cued; R cueing, radial-depth cueing; Z cueing, Z-depth cueing.

1047-8477/97 $25.00

raphy for analyzing virus particles and other macromolecular complexes at moderate to high resolutions (Booy *et al.*, 1994; Kühlbrandt *et al.*, 1994; Zhou *et al.*, 1994; Cheng *et al.*, 1995; Morgan *et al.*, 1995; Stark *et al.*, 1995; Baker and Cheng, 1996; Conway *et al.*, 1996). We recently applied these methods to mammalian reovirus particles (Dryden *et al.*, 1993). In an effort to extract new information from existing datasets, we tested different techniques provided by the IRIS Explorer software (Numerical Algorithms Group, Chicago, IL) (Halse, 1992) for visualizing the reconstructions.

Diverse visual cues can aid in interpreting computer-generated images of macromolecules (Namba *et al.*, 1988). Since structures determined by cryo-TEM and image reconstruction are rendered by computer as 3-D isosurfaces, but displayed in only two dimensions (van Heel, 1983; Radermacher and Frank, 1984), one or more lighting effect is added to manifest the object's 3-D nature. Commonly, an isosurface is rendered as though broadly illuminated by a light over one of the viewer's shoulders, causing the surface to be marked by shadows. This effect, surface shading, is essential for perceiving the topography of the isosurface. For larger structures, a second effect is often added to indicate the object's depth, namely, the isosurface is rendered as though a spotlight were directed toward its center along the *Z* axis. This effect, called Z cueing in this article, produces a gradient of shades that extends from front to back of the object. Van Heel (1983) and Radermacher and Frank (1984) used Z cueing in early work with cryo-TEM and image reconstruction, and Z cueing has since been widely applied, particularly to reconstructions of virus particles (e.g., Fuller, 1987; Schrag *et al.*, 1989; Booy *et al.*, 1994; Prasad *et al.*, 1994; Yeager *et al.*, 1994; Baker and Cheng, 1996; Conway *et al.*, 1996). Despite its widespread use, Z cueing has limitations for interpreting the symmetrical arrangements of protein subunits on the surfaces of virus particles or for understanding more internal structures.

Color has also been used to enhance display of structures solved by cryo-TEM and 3-D image reconstruction. In some cases, color coding has been obtained by truncating a cryo-TEM dataset by difference mapping with another dataset and then specifying the region of the difference map to be rendered in a distinct hue (Booy *et al.*, 1994; Yeager *et al.*, 1994). Similarly, icosahedral virus particles have been rendered so that structures over defined ranges of radii have distinct colors, producing radially depth-cued (R-cued) images (Schrag *et al.*, 1989; Yeager *et al.*, 1994). Other methods for rendering specific portions of a structure in distinct shades have also been used (Akey and Radermacher, 1993; Cheng *et al.*, 1995; Conway *et al.*, 1996). A common aspect of these techniques is that they provide the viewer with cues for perceiving important features of the complex structures.

Namba *et al.* (1988) described a related method to enhance displays of macromolecules, in which a smooth gradient of color is added to provide radial-depth cueing (R cueing) from the center of quasi-spherical structures (e.g., icosahedral viruses) or from the central axis of quasi-cylindrical structures (e.g., helical filaments). Salunke *et al.* (1989) used this same style of R cueing in a computer-created model for polyomavirus virions. More recently, Grant *et al.* (1992) used radial color gradients to highlight topographical features on the surfaces of small icosahedral viruses analyzed by X-ray crystallography. Other methods to provide R cueing of virus particles displayed from atomic coordinates were described by Sgro (1996). Very recently, Chiu, Prasad, and colleagues have applied R cueing with color gradients to several structures of virus particles newly determined by cryo-TEM and image reconstruction (e.g., Thurman-Commike *et al.*, 1996; Prasad *et al.*, 1996; Lawton *et al.*, 1997). Color gradients have also been applied to cross-sectional images from cryo-TEM reconstructions to demonstrate electron density distributions (Griffith *et al.*, 1992; Dryden *et al.*, 1993; Cheng *et al.*, 1995).

In this study, we used the IRIS Explorer software to apply radial color maps to reconstructions of mammalian reovirus particles derived by cryo-TEM (Dryden *et al.*, 1993). New insights into structure–function relationships in these particles were obtained. To demonstrate the utility of this approach with other icosahedral structures, we applied similar styles of R cueing to reconstructions of human rhinovirus (Olson *et al.*, unpublished), cowpea chlorotic mottle virus (Speir *et al.*, 1995), and the pyruvate dehydrogenase complex from *Saccharomyces cerevisiae* (Stoops *et al.*, 1992). Using a reconstruction of the flagellar filament from *Salmonella typhimurium* (Morgan *et al.*, 1995), we showed that the methods can be applied to helical structures with comparable benefits. We conclude that depth cueing with radial color gradients provides a useful tool for displaying macromolecular structures of different symmetries.

MATERIALS AND METHODS

Rendering Isosurfaces

Visualization was performed on a Silicon Graphics Indigo^2 workstation (cpu: R4400, 150 MHz; graphics: XZ; memory: 160 MB; virtual memory: 400 MB) using IRIS Explorer 2.2, an application-builder software package that contains a library of distinct subroutines (modules) (Halse, 1992). Modules were connected to form customized programs (maps, Fig. 1), which were executed to produce visualizations. Explorer implements the

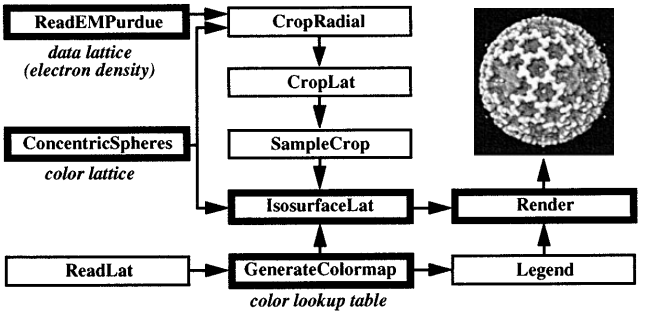

FIG. 1. A map constructed with IRIS Explorer 2.2 (Numerical Algorithms Group, Chicago, IL) and used to render R-cued isosurfaces. Individual modules (rectangles) are connected in an ordered fashion (arrows) to create the complete map. Essential modules are indicated by bold boxes. The functions of each module are described in the text (Materials and Methods). The modules ReadEMPurdue, ConcentricSpheres, and GenerateColormap provide three distinct types of data to the IsosurfaceLat module as shown in italics.

marching cubes algorithm for calculating isosurfaces (Cline *et al.*, 1988). It can be run under operating systems from various computer manufacturers (Silicon Graphics, Sun Microsystems, Digital Equipment Corporation, International Business Machines, Hewlett Packard) and is also available for computers running the Windows NT (Microsoft) operating system.

At the outset of this work, we used the program DataScribe, a part of the IRIS Explorer package, to create a new module, ReadEMPurdue, to convert cryo-TEM datasets generated at Purdue University (reovirus, rhinovirus, pyruvate dehydrogenase, and CCMV) from ASCII format to a format supported by Explorer 2.2. We designed this module so that it extracted not only the density values assigned to each voxel in the 3-D array but also the size of the array from the data header and then exported this data as a uniform 3-D data lattice. A related program (ReadEMBrandeis) was created to convert the cryo-TEM dataset for the flagellar filament generated at Brandeis University from ASCII to Explorer format.

Within Explorer, we began by assembling a minimal map, connecting the ReadEMPurdue (or ReadEMBrandeis) module to the IsosurfaceLat module, which calculates the isosurface, and connecting the IsosurfaceLat module to the Render module, which renders the image (Fig. 1). Isosurfaces were generated by launching the mapped program after routinely setting the density contour (controlled by the IsosurfaceLat module) at two to four times the noise level (e.g., Belnap *et al.*, 1996), at which level the molecular envelope of known structures closely approximates the expected molecular mass and faithfully fits atomic structures determined by x-ray crystallography (e.g., Belnap *et al.*, 1996; Conway *et al.*, 1996; Trus *et al.*, 1997). The Render module also applies lighting effects to rendered objects, thus providing surface-shaded representations, and permits structures to be manipulated in several ways upon rendering, including rotation and changes in size (Halse, 1992).

Additional modules were inserted between the ReadEMPurdue and IsosurfaceLat modules (Fig. 1) to permit the data lattices to be resampled before rendering, both to expedite the rendering process and to aid in analyzing the structures. For example, we routinely inserted the Explorer SampleCrop module, which permits a data lattice to be reduced in resolution during preliminary stages of the visualization process by sampling a uniformly distributed subset of voxels from the whole dataset and to be sectioned by planes along the *X*, *Y*, and/or *Z* axes. Since the SampleCrop module cuts through the isosurface skin of a particular density value, the cropped structures appear hollow, thus, we created and inserted a new module, CropLat, which permits sectioning in the *X*, *Y*, and/or *Z* directions and also permits the sectioned faces to be rendered as apparently filled structures (see Figs. 2 and 3 for examples of use). We also created and inserted the new module RadialCrop, which operates similarly to CropLat but permits sectioning in the radial direction (see Fig. 5 for an example of use). RadialCrop also requires input from the ConcentricSpheres or ConcentricCylinders module described below. Other modules were inserted to provide R cueing (see below).

R Cueing

R cueing was applied to the isosurfaces by texture mapping, a rendering technique supported by the IsosurfaceLat module of IRIS Explorer 2.2 (Halse, 1992). With this method, a value is assigned to each voxel in the full 3-D array comprising a color lattice that is separate from the lattice of electron density values (data lattice). The color lattice is given a defined shape (spherical or cylindrical in this study), and color values are then assigned according to a color lookup table, or colormap.

To generate the shape-defined color lattices required for this work, we employed the Shape Language, an array manipulation language that can be used by the LatFunction module of IRIS Explorer 2.2, to create two more custom modules. For rendering icosahedrally symmetrical structures, we created the new module ConcentricSpheres, which generates a color lattice consisting of a 3-D array of concentric, radially defined spheres whose total size is adjustable to the size of each data lattice. For rendering helically symmetrical structures, we created the new module ConcentricCylinders, which generates a color lattice consisting of a 3-D array of concentric cylinders whose total size is adjustable to the size of each data lattice. (Note that IRIS Explorer 3.0, which was released in April 1995, contains the new module RadialLat which is comparable in function to the ConcentricSpheres module.)

Colormaps for assigning values to the color lattice were generated with the GenerateColormap module of IRIS Explorer 2.2. To arrive at the desired color scheme for a structure, we used the GenerateColormap module to specify hue, saturation, and value (HSV mode) for all radii. In this report, we refer to variations in either saturation alone or in saturation and value together as variations in "brightness." Several different types of colormaps were used, as summarized in Table 1. To give an example, the single-hue colormap applied to the reovirus ISVP in Fig. 2 was generated by adjusting hue to remain a constant blue over the full range of radii; saturation to change in an approximately linear

TABLE I

Types of Colormaps Used in Generating R-Cued Images in This Study

Type of colormap	Settings for:	
	Hue	Brightness[a]
Single-hue	Kept constant	Changed continuously with radius[b]
Spectral	Changed continuously with radius[b]	Kept constant
Stepped-hue	Changed at discrete radii in a discontinuous manner	Changed continuously with radius within each step

[a] We defined brightness as a combination of saturation and value in the HSV mode of rendering in IRIS Explorer.

[b] The rate at which hue or brightness was changed as a function of radius within a given structure was sometimes varied to enhance discrimination of particular features.

fashion over a relevant subset of radii (20–40 nm); and value to remain constant at full intensity over the entire range of radii. Stepped-hue colormaps were routinely generated by adjusting hue to remain constant over wide subsets of relevant radii, saturation to change in an approximately linear fashion over each subset, and value to remain constant at full intensity over the entire range of radii. Spectral colormaps were routinely generated by adjusting hue to change in an approximately linear fashion over a relevant subset of radii and both saturation and value to remain constant at full intensity over the entire range of radii. More complex colormaps were also used as described in the text.

To render R-cued images, we modified each Explorer map (Fig. 1) by connecting the ConcentricSpheres or ConcentricCylinders module, which generates the color lattice, to the IsosurfaceLat module. To the IsosurfaceLat module we also connected the GenerateColormap module, which assigns color values to each voxel in the color lattice. Routinely, we also added to the map a ReadLat module, to recall a previously generated colormap, and a Legend module, to display the relationship between radius and color (see color bars in Figs. 2–4).

Final Images

Rendered images were obtained by screen capture from the Silicon Graphics Indigo^2 workstation. The image files were then opened in Photoshop 3.0 (Adobe Systems) on a Macintosh computer (Apple Computer, Inc., Cupertino, CA) to make final adjustments to the hue, saturation, magnification, and resolution of each image and to assemble figures. Prints were generated by exporting files to a Phaser 440 printer (Tektronix, Wilsonville, OR).

RESULTS AND DISCUSSION

R Cueing with the Reovirus ISVP

We used different styles of depth cueing to render image reconstructions of mammalian reovirus particles (Dryden *et al.*, 1993). Findings are illustrated for surface-shaded isosurfaces of the infectious subvirion particle (ISVP) in Figs. 2a–2d. Traditional schemes involved either no cueing besides surface shading (Fig. 2a), Z cueing, or both (Fig. 2b). Other schemes involved R cueing (Figs. 2c and 2d) and utilized different types of colormaps (Halse, 1992) including single-hue colormaps with a smooth gradient of shades (Fig. 2c) and stepped-hue colormaps (Fig. 2d) as described below. Cross sections (Figs. 2e and 2f) demonstrate that the colormaps were applied as a function of radius in the last two cases.

The images indicate that R cueing can enhance the discrimination of elements that occupy radially or symmetrically equivalent positions in an object because these elements are color-coded in a consistent fashion. This fact is exemplified by the star-like pentamers of protein λ2 that are exposed on the ISVP surface at its 12 icosahedral vertices (Dryden *et al.*, 1993). In the image that was R-cued with a single-hue colormap (Fig. 2c), it is easy to see that each of the λ2 pentamers (light blue) is similarly inset relative to the trimeric heads of protein μ1 (white) that are arranged over the remaining surface (Dryden *et al.*, 1993). This feature is less apparent with other styles of cueing (Figs. 2a and 2b).

Reovirus particles are multilayered structures, comprising two concentric protein capsids and a central mass of double-stranded (ds)RNA (Nibert *et al.*, 1996; Dryden *et al.*, 1993). To code for this layering, we used a stepped-hue colormap in which smooth gradients of a single hue were applied within layers, but hues were discontinuously shifted between layers (Figs. 2d and 2f). With the more complicated colormap, it is readily evident that solvent channels completely penetrate the outer capsid so that portions of the inner capsid (magenta) are exposed at their bases (Fig. 2d). The enhanced presentation of the ISVP in Fig. 2d demonstrates that once important features of a structure are known, the colormap can be modified to highlight these features, a procedure we call colormap optimization.

Colormap Optimization with Other Icosahedral Structures

To assess the general utility of radial color gradients, we studied other icosahedral structures solved by cryo-TEM and image reconstruction. Three distinct types of colormaps were used to accentuate features of each structure (Table 1): single-hue colormaps, in which hue was kept constant and brightness was varied as a function of radius; spectral colormaps, in which brightness was kept constant and hue was varied as a function of radius; and stepped-hue colormaps, in which hue was kept constant over a wide range of radii but abruptly shifted to a new hue at one or more selected radius. In stepped-hue colormaps, brightness was usually varied as a function of radius over the range of radii for each hue.

Human rhinovirus. In addition to its analysis by X-ray crystallography (Rossmann *et al.*, 1985), the structure of human rhinovirus type 14 (HRV14) was determined to a resolution of 22 Å by cryo-TEM and image reconstruction (Olson *et al.*, unpublished). We examined this pseudo $T = 3$ structure by R cueing with a goal of highlighting the features on its surface with known significance in infection and host response (reviewed in Rueckert, 1995). We found that a single-hue colormap was useful in this regard, as its simplicity allowed the overall topography of the single capsid of this virus to be readily perceived (Fig. 3a).

Three regions on the surface of HRV14 were made evident by R cueing as previously emphasized in images produced from atomic coordinates (Grant *et al.*, 1992; Sgro, 1996). (1) Centered at the fivefold axes are densities that project outward to the greatest radial extent (lightest blue in Fig. 3a) and form star-shaped mesas. These areas include NIm-IA and NIm-IB, two of four antigenic regions that are recog-

nized by neutralizing antibodies (Rossmann *et al.*, 1985; Sherry *et al.*, 1986). (2) Centered at each of the threefold axes is another projecting density, shaped like a right-handed pinwheel, the highest areas of which (light blue in Fig. 3a) occur at the pinwheel tips and extend as an L-shaped ridge to the threefold axis. These areas include the other two regions recognized by neutralizing antibodies, NIm-II and NIm-III (Rossmann *et al.*, 1985; Sherry *et al.*, 1986). (3) Outlining the five- and threefold densities is a network of depressions (darker blue in Fig. 3a). These depressions include a region named the canyon (C in Fig. 3a) (Rossmann *et al.*, 1985), which represents the site where the cell-surface receptor for the major group of human rhinoviruses, ICAM-1, binds to the capsid surface (Olson *et al.*, 1993).

Truncated core of the pyruvate dehydrogenase complex. To extend the application of R cueing to an icosahedrally symmetrical, but nonviral, structure, we studied the core of the pyruvate dehydrogenase (PDH) complex from *S. cerevisiae* (reviewed in Reed and Hackert, 1990). The structure of the PDH core was solved to a resolution of 25 Å by cryo-TEM and image reconstruction and consists of 60 identical subunits that are grouped as trimers at the vertices of a cage-like dodecahedron (Stoop *et al.*, 1992). While single-hue radial colormaps provide an uncomplicated way to gauge external surfaces, we found that they are less useful for more open structures like this one. Instead a spectral colormap, which furnishes a greater range of distinguishable colors, was more effective for discriminating structural elements over the wide range of radii in the PDH core (Fig. 3b).

Each trimer in the PDH core is shaped like a cone, with a flattened base outside (purple in Fig. 3b) and a pointed apex inside (orange in Fig. 3b). Adjacent trimers make contact across bridges at the twofold axes (cyan as viewed externally in Fig. 3b). R cueing helps especially in displaying the internal structure of this complex, where the 20 trimer apices project toward the center of the dodecahedron.

Native and swollen forms of cowpea chlorotic mottle virus. To test R cueing for comparing structures related by conformational changes, we studied the native and swollen forms of the $T = 3$ cowpea chlorotic mottle virus (CCMV). The transition of CCMV from native to swollen occurs *in vitro* upon removal of Ca^{2+} ions and mimics a process that occurs in the plant cytoplasm as infection is initi-

FIG. 2. The ISVP of mammalian reovirus type 1 Lang as determined by cryo-TEM and 3-D image reconstruction (Dryden *et al.*, 1993). (a–d) Surface-shaded representations. The representations are identical except for the style of depth cueing that was imposed on the isosurface. Surface shading is applied to each representation as though a light were directed at the object from over the viewer's left shoulder. (a) No additional depth cueing. Features representing outer capsid proteins λ2, μ1, and σ1 and channels P2 and P3 (Metcalf *et al.*, 1991) are labeled. The μ1 protein is primarily present as fragments μ1N and μ1C in virions and as fragments μ1N, δ, and ϕ in ISVPs (Nibert and Fields, 1992). Only the base of the σ1 fiber protein (Furlong *et al.*, 1988) is visible in the virion and ISVP reconstructions (Dryden *et al.*, 1993). (b) Z cueing. Color is a function of distance from the viewer. Hue remains constant, but brightness decreases as distance from the viewer increases. (c) R cueing, single-hue colormap. Color is a function of distance from the particle center (see color bar; r, radius, in nm). Hue remains constant, but brightness decreases as distance from the center decreases. (d) R cueing, stepped-hue colormap. Color is a function of distance from the particle center (see color bar; r, radius, in nm). A sharp transition in hue was introduced near radius 30 nm to approximate the boundary between outer capsid (blue) and inner capsid (magenta). Another sharp transition in hue was introduced near radius 23.5 nm to approximate the boundary between inner capsid (magenta) and genomic dsRNA (yellow). Across the radii of blue or magenta hue, brightness decreases as distance from the particle center decreases. (e, f) R-cued representations of the reovirus ISVP, cropped to remove the front half of the particle as viewed along a twofold axis. Only the top half of the cross section is shown. (e) Single-hue colormap, same as in (c). (f) Stepped-hue colormap, same as in (d).

FIG. 3. R-cued images of other macromolecular structures as determined by cryo-TEM and image reconstruction. All images are shown to approximate scale: the white bar at top indicates 10 nm. (a) Surface-shaded representation of human rhinovirus 14 (Olson *et al.*, unpublished) shown in stereo. R cueing was performed using a single-hue colormap, with approximate radial distances indicated (see color bar; r, radius, in nm). Antibody-binding protrusions (NIm sites IA, IB, II, and III) and receptor-binding canyon (C) are labeled. (b) Surface-shaded representation of the truncated core of the pyruvate dehydrogenase complex from *Saccharomyces cerevisiae* (Stoops *et al.*, 1992) shown in stereo. R cueing was performed using a spectral colormap, with approximate radial distances indicated (see color bar; r, radius, in nm). (c–f) Representations of the native and swollen forms of cowpea chlorotic mottle virus (Speir *et al.*, 1995). (c, d) Surface-shaded representations of the native (c) and swollen (d) forms. (e, f) 2-nm-thick central slices of native (e) and swollen (f) forms. An identical spectral colormap was used for all these representations, with approximate radial distances indicated (see color bar; r, radius, in nm). The colormap included sharp changes in hue or brightness near radii 13 and 14.5 nm, respectively (described in the text), to highlight the different elevations of the pentameric (P) and hexameric (H) capsomers in both native and swollen forms. (g–i) A portion of the flagellar filament of *Salmonella typhimurium* (Morgan *et al.*, 1995). (g) Surface-shaded representation shown in stereo. By convention, the filament (a left-handed helical structure in its wild-type form) is viewed in profile as though extending from the surface of a bacterium above it (Trachtenberg and DeRosier, 1991). (h) Longitudinal cross section, same orientation as in (g). (i) Transverse cross section, 2-nm thick and viewed as though looking toward the bacterium. Features that represent domains of the flagellin subunits (D1–3) are labeled. An identical stepped-hue colormap was applied in these representations, with approximate radial distances indicated (see color bar; r, radius, in nm). A transition in hue from salmon to orange was introduced near radius 7 nm to distinguish the two nodular subdomains of domain D2. A second transition in hue was introduced near radius 3 nm to distinguish the D1 domain (dark orange) from the ring of density (yellow) that surrounds the central channel. Across the radii of salmon, orange, or yellow hue, brightness was made either to decrease (salmon and orange) or to increase (yellow) as distance from the helical axis decreases.

ated. Structures of native and swollen virions were solved to a resolution of 28 Å by cryo-TEM and image reconstruction (Speir *et al.*, 1995). We found that a spectral colormap was effective for interpreting the more open structure of swollen CCMV (Figs. 3d and 3f) and comparing it to the native form (Figs. 3c and 3e).

In native CCMV virions, external regions of the 180 coat protein subunits associate to form hexameric and pentameric capsomers (blue to cyan in Fig. 3c), each of which surrounds a central channel and projects from lower regions of the capsid surface (blue–green in Fig. 3c). As seen in cross sections (Fig. 3e), native virions also contain a distinct layer of inner density (yellow to red), which includes both the genomic plus-strand RNA and an RNA-binding domain of each capsid subunit (Speir *et al.*, 1995). R cueing reveals that these internal structures are exposed through the central channels of both hexameric (Fig. 3c) and pentameric (barely visible in Fig. 3c) capsomers.

After swelling, significant changes are observed throughout the CCMV virion. The diameter of the particle increases by nearly 2 nm, which is demonstrated by the radial expansion of outer portions of both hexameric and pentameric capsomers into more

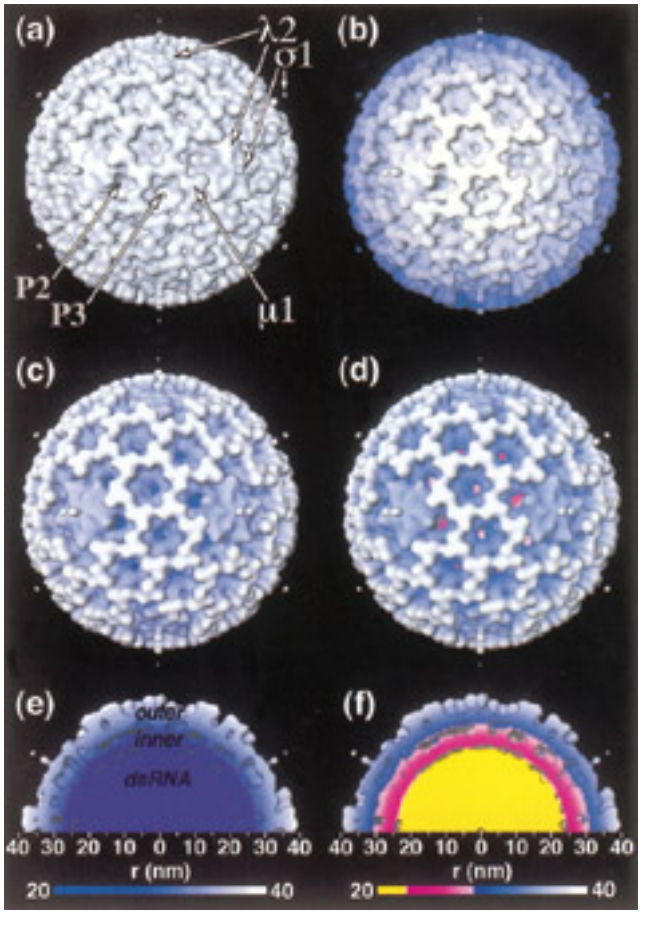

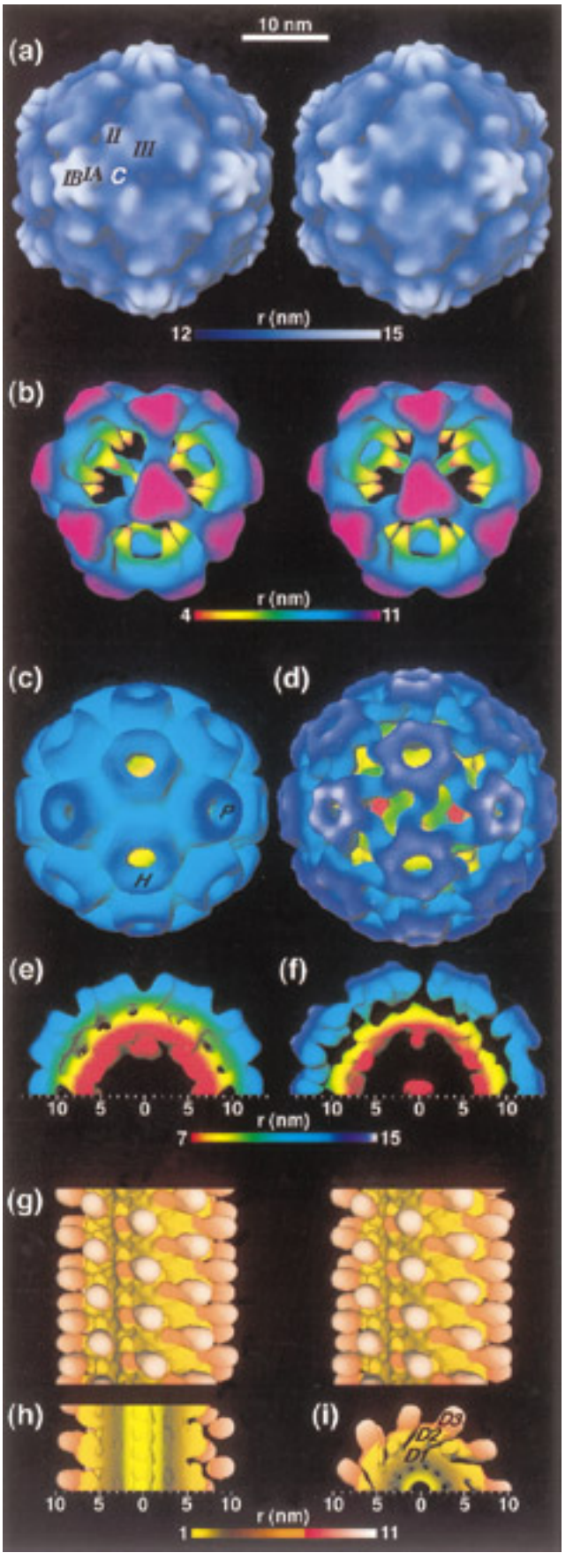

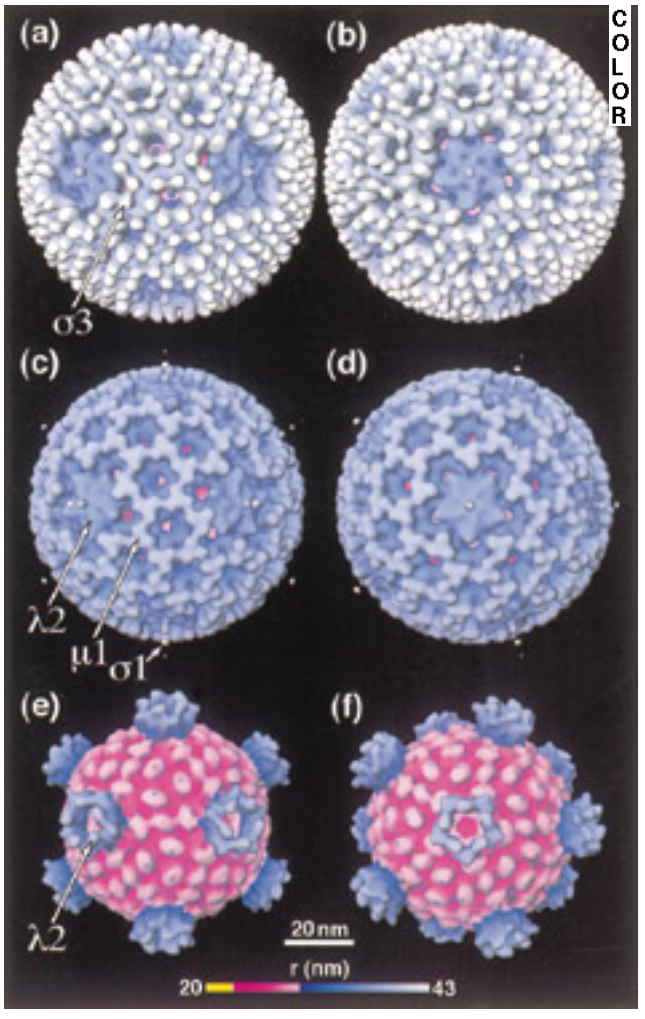

FIG. 4. R-cued, surface-shaded representations of different particle forms of mammalian reovirus type 1 Lang, as determined by cryo-TEM and image reconstruction (Dryden *et al.*, 1993). (a, b) Virion. (c, d) ISVP. (e, f) Core. Each particle is viewed down both twofold (a, c, e) and fivefold (b, d, f) axes of symmetry. The same stepped-hue colormap was applied to all these representations, with approximate radial distances indicated (see color bar; r, radius, in nm). As in Fig. 2, the structural layers are coded as follows: outer capsid in blue, inner capsid in magenta, and dsRNA in yellow. Features representing outer capsid proteins λ2, μ1, σ1, and σ3 are labeled. See the legend to Fig. 2 for clarifications about the μ1 and σ1 proteins. White scale bar, 20 nm.

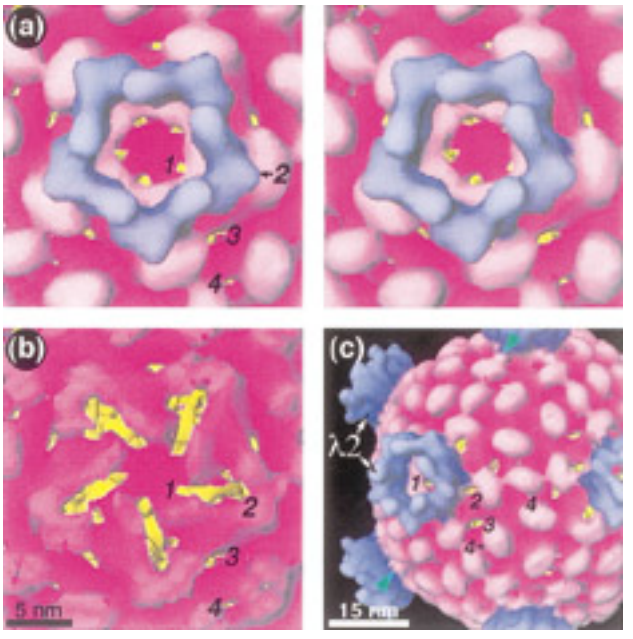

FIG. 5. R-cued representations of the core of reovirus type 1 Lang, displayed at an increased density contour. The stepped-hue colormap applied in these representations is identical to that in Fig. 4. Pores through the inner capsid (labeled 1–4 according to type) reveal dsRNA in yellow beneath them. (a) Closeup of the λ2 pentamer, surface-shaded representation shown in stereo. The pentamer is viewed down the axis of fivefold symmetry in (a, left). Each pore 2 is obscured by a λ2 subunit when the particle is viewed down a fivefold axis (truncated arrow points to its position in (a, left). (b) Same view as in (a, left), but with the structure cropped above radius 28 nm so that most or all of each λ2 subunit is excluded from view. (c) Surface-shaded representation, viewed down a twofold axis. Turrets of protein λ2 are labeled. Green arrowheads highlight where the blue–magenta transition in the colormap appears to transect the λ2 subunits. Black scale bar in (b), which also applies to (a), 5 nm. White scale bar in (c), 15 nm.

violet regions of the colormap (Figs. 3d and 3f). The capsid subunits also pull away from each other, opening large channels at the quasi-threefold axes (Speir *et al.*, 1995), through which internal structures can be viewed (Fig. 3d). Swelling also affects the inner layer of protein and RNA in CCMV particles: this layer moves radially outward into more yellow–green regions of the colormap and is also thinned, perhaps reflecting its increased circumference (Fig. 3f).

A complexity was added to the colormap to highlight another feature that is common to both native and swollen CCMV. As we studied these structures during colormap optimization, we noted that the pentameric subunits extend to a slightly greater radius (by <0.5 nm) than the hexameric subunits, as would occur if the subunits were arranged in a capsid whose morphology is slightly icosahedral (i.e., nonspherical). This small difference proved difficult to demonstrate with linearly progressive colormaps, but by sharply shifting either hue or brightness at appropriate radii for the two particles, we were able to improve its visualization. Thus, pentamers extend into more blue–violet regions than do hexamers in native CCMV (Fig. 3c) and into whiter regions than do hexamers in swollen CCMV (Fig. 3d).

R Cueing and Colormap Optimization with a Helical Structure

R cueing can also be used with structures that are arranged about an axis of symmetry (Namba *et al.*, 1988). We applied R cueing to the helically symmetri-

cal flagellar filament of *S. typhimurium*, the structure of which was determined to a resolution of 11 Å by cryo-TEM and image reconstruction (Morgan *et al.*, 1995). In this case, the color lattice was first adjusted to the shape of a cylinder (see Materials and Methods), and gradients of color were applied according to radial distance from the cylinder axis. We found that a stepped-hue colormap was necessary to visualize many of the important features of the flagellar filament (Figs. 3g–3i).

The flagellin subunits in the filament are divided into at least three domains, designated D1–3 (DeRosier, 1992; Namba *et al.*, 1989). R cueing, in combination with stereoscopic display, substantially simplifies visualization of the two more external domains, D2 and D3, in visually complex surface renditions of the flagellar filament (Fig. 3g). In addition, by introducing a transition in color (salmon to orange) near a radius of 7 nm, we were able to demonstrate that the two subdomains of D2 (DeRosier, 1992) extend to different radial heights (one salmon, the other orange) and alternate axially along the filament surface (Fig. 3g), which allows the viewer to discriminate that each of the D2 domains is elongated in an axial direction. We introduced another transition in hue (orange to yellow) near a radius of 3 nm to distinguish the D1 domain (dark orange) from a ring of distinct density (yellow) that is visible surrounding the central channel in cross sections of this structure (Figs. 3h and 3i) and has been attributed to a set of α-helices that run parallel to the helix axis (Morgan *et al.*, 1995).

Extending Structure–Function Studies of Mammalian Reovirus Particles

Having defined the utility of different styles of R cueing for analyzing structures solved by cryo-TEM and image reconstruction, we applied these methods toward extracting new information from the structures of reovirus particles. Our primary goal was to understand how these structures reflect the mechanisms of reovirus entry of cells and transcription of its genome by particle-associated enzymes.

Conformational changes between virions, ISVPs, and cores. Dramatic structural changes occur between the different particle forms—virions, ISVPs, and cores (Fig. 4)—of mammalian reoviruses (Nibert *et al.*, 1991; Dryden *et al.*, 1993; Nibert and Fields, 1994). These changes result from a combination of events that involve outer capsid proteins λ2, μ1, σ1, and σ3 and include conformational changes (Dryden *et al.*, 1993; Furlong *et al.*, 1989), proteolytic cleavages (Nibert and Fields, 1992), and elutional losses (Dryden *et al.*, 1993). The changes in structure are accompanied by equally dramatic changes in function with respect to the three primary steps in reovirus entry: attachment, membrane penetration, and transcriptase activation (reviewed in Nibert and Fields, 1994).

We used R cueing with a stepped-hue colormap to enhance display of the structural changes that accompany reovirus entry. The progressive exposure of deeper structures is revealed by changes in surface color between virions (Figs. 4a and 4b), ISVPs (Figs. 4c and 4d), and cores (Figs. 4e and 4f). Loss of σ3 from virions exposes the darker blue regions of μ1 that surround the P2 and P3 channels in ISVPs (refer to Fig. 2a for channel positions), and loss of μ1 from ISVPs exposes much of the magenta inner capsid in cores. In addition, use of a stepped-hue colormap eases recognition that the inner capsid is exposed through the P2 and P3 channels in both ISVPs and virions. In contrast, the stepped-hue colormap reveals that RNA (yellow) is not clearly exposed through the inner capsid layer in cores, at least not at the resolution of these datasets or at the density contour chosen for this display, indicating that the inner capsid is not penetrated by such large solvent channels as the outer capsid (Dryden *et al.*, 1993).

Core nodules. From published data, it is unclear whether the two-, three-, and fivefold-related nodules on the core surface have the same or different compositions (Metcalf *et al.*, 1991; Dryden *et al.*, 1993). By carefully choosing the radius near 30 nm at which a transition in hue was introduced (Figs. 4e and 4f), we found that these nodules extend to slightly different maximum radii ($<$0.5 nm separation). The threefold-related nodules extend to the highest radius (blue tips in Figs. 4e and 4f), the fivefold-related nodules to the lowest radius (fully magenta tips in Figs. 4e and 4f), and the twofold nodules to an intermediate radius (faint blue tips in Figs. 4e and 4f). Since it is difficult to explain these observations by concluding that the core shell exhibits some type of nonspherical morphology, the observations may suggest that the three types of nodules have different organizations, perhaps involving different proteins or different regions of the same proteins. Proteins λ1 and σ2 are the best candidates to form the core nodules (Xu *et al.*, 1993).

The fivefold-related nodules make contact near one end with the base of the λ2 turrets (Dryden *et al.*, 1993) (Fig. 4e), and this feature highlights one complication of R cueing with stepped-hue colormaps. If the components of one or both layers of a structure interdigitate radially and if a sharp transition in hue is used to approximate the boundary between layers, then the hue transition must transect some of the interdigitating components. This seems to have occurred with λ2 in Figs. 4 and 5: the transition in hue appears to transect each λ2 subunit so that most of λ2 is blue but a region at its base is

magenta (e.g., green arrowheads in Fig. 5c). Additional studies are needed to determine which densities near the base of the λ2 turret, including the light magenta shelf visible within the pentamer channel (Figs. 4f and 5a), are attributable to λ2 itself and which to other components of the inner capsid.

Sites of mRNA export by transcribing cores. Cores contain the enzymes needed to generate full-length mRNAs from the 10 genomic dsRNA segments; to add a eukaryotic cap 1 structure to their 5′ ends; and to export them into the cytoplasm of an infected cell (reviewed in Nibert *et al.*, 1995). Based on electron micrographs of transcribing cores, mRNA export was proposed to occur through the pentamers of protein λ2 that project from the core surface (Bartlett *et al.*, 1974). More recent observations suggest that the enzymes that mediate transcription, capping, and export of reovirus mRNAs colocalize to the fivefold axes of cores, at the base of the λ2 pentamers (Mao and Joklik, 1991; Koonin, 1993; Starnes and Joklik, 1993; Dryden, K.A., *et al.*, submitted for publication). Nevertheless, published images of cores have not revealed any holes through the inner capsid through which the nascent mRNAs might be exported during transcription (Dryden *et al.*, 1993; Metcalf *et al.*, 1991). One possibility is that these holes are so small that they are obscured in the current electron density map (32-Å resolution). Another is that the holes are not opened until conformational changes in the core that accompany active transcription (Powell *et al.*, 1984). In either case, we might expect the sites of mRNA export to be represented by regions of lower density in the current map of the inner capsid of nontranscribing cores.

In an effort to visualize such regions, we utilized R cueing to scrutinize the core. By gradually increasing the contour level from that normally used to depict cores (Figs. 4e, 4f, and 5; contour set at four times the noise level), we observed several types of holes through the inner capsid, that is, small regions through which the genomic RNA (coded yellow in the stepped-hue colormap) was visible from outside the particle (labeled 1–4 in Fig. 5; contour set at six times the noise level). One type of hole (labeled 1) was visible within the channel of the λ2 pentamer. Upon further inspection, we recognized that this and another hole found just outside the λ2 pentamers (labeled 2 but obscured in Fig. 5a) might be parts of a larger feature. This fact was confirmed by cropping the core to a radius of 28 nm, at which point the λ2 knobs were removed from the image, revealing a trough that runs beneath each λ2 subunit (Fig. 5b).

Although the significance of these features remains unproven, they may relate to RNA transport during reovirus transcription. The regions of lower density around the base of each λ2 pentamer are reminiscent of holes at identical symmetry positions in the inner capsid (VP2) layer of rotaviruses (Lawton *et al.*, 1997). In rotaviruses, these holes were recently proposed to be the sites through which the viral mRNAs are extruded during transcription by the viral RNA polymerase complex (Lawton *et al.*, 1997), which is attached beneath the VP2 layer at the fivefold axes of symmetry (Prasad *et al.*, 1996). Our own recent data similarly suggest that a protein complex that includes the reovirus RNA polymerase protein λ3 projects into the particle interior beneath each λ2 turret in reovirus cores (Dryden, K. A., *et al.*, submitted for publication). The magenta surface that forms the base of the λ2 channel (Figs. 4 and 5) probably represents the most radial aspect of this complex. Other recent data from cryoelectron microscopy and 3-D image reconstruction of transcribing cores suggest that reovirus transcripts are indeed extruded through the λ2 channel and that subtle rearrangements near the base of λ2 accompany active transcription (Yeager *et al.*, 1996). The trough-like features beneath λ2 seen here (Fig. 5b) may be paths along which product or template RNAs are threaded toward or away from the transcriptase complex (Dryden *et al.*, submitted for publication). That the sites we postulate for mRNA export are found at the periphery of the λ2 pentamer channel, and not at its center, is attractive in that if the 5′ ends of the mRNAs were extruded through the center of the channel, they would have to diffuse laterally by ≥2.5 nm (Dryden *et al.*, 1993) to access the mRNA capping enzyme(s) associated with λ2 (Mao and Joklik, 1991). Such an arrangement could make for an inefficient capping process; however, if our interpretations are correct and the mRNAs are extruded through more peripheral sites, then they emerge from the particle interior in close proximity to λ2, well positioned for capping.

R Cueing as a Pedagogical Tool

Extracting information from printed or projected images of macromolecules can be challenging for both professional and amateur biologists. This becomes more true as the structures increase in size and complexity, as with virus particles and other large assemblies. Both research and educational goals dictate that investigators use visualization methods that make relevant structural details as accessible to viewers as possible. We have found R cueing with continuous or discontinuous color gradients to be one such technique that enhances the presentation of large macromolecular structures solved by cryo-TEM and image reconstruction. It should be noted, however, that R cueing as described here may not be optimal for rendering objects whose morphology is highly asymmetric (e.g., Frank, 1997)

or in which equivalent or quasi-equivalent subunits lie at significantly different radii (e.g., Bottcher *et al.*, 1997).

In this article we have emphasized the use of color gradients for portraying radial depth in icosahedral virus particles and other macromolecular assemblies. Nonetheless, R cueing can also enhance visualizations of structures in grayscale, that is, if appropriate considerations are given to obtaining proper contrast in different parts of the structures. For evidence, the reader is referred to the small image in Fig. 1 of this article and to Figs. 2m–2o in Centonze *et al.* (1995).

We thank J. Walton of Numerical Algorithms Group, Ltd., United Kingdom, for providing the Shape Language program to generate spherical arrays and D. G. Morgan and D. J. DeRosier for sharing their cryo-TEM dataset for the flagellar filament of *Salmonella typhimurium*. We also thank D. M. Belnap, R. B. Inman, R. R. Rueckert, and S. B. Walker for helpful discussions and D. M. Belnap, D. L. Farsetta, D. G. Morgan, S. Noble, R. R. Rueckert, and L. A. Schiff for reviewing portions of the manuscript before submission. S.M.S. and J.Y.S. were supported by a grant from the Lucille P. Markey Charitable Trust to the Institute for Molecular Virology (The Graduate School, University of Wisconsin-Madison). M.L.N. was additionally supported by N.I.H. Grant R29 AI39533, A.C.S. Grant IRG-35-37-7, and a Shaw Scientists Award from the Milwaukee Foundation (Milwaukee, WI). T.S.B. was supported by N.I.H. Grant R01 GM33050 and N.S.F. Grant MCB9527131.

REFERENCES

Akey, C. W., and Radermacher, M. (1993) Architecture of the *Xenopus* nuclear pore complex revealed by three-dimensional cryo-electron microscopy, *J. Cell Biol.* **122,** 1–19.

Baker, T. S., and Cheng, R. H. (1996) A model-based approach for determining orientations of biological macromolecules imaged by cryoelectron microscopy, *J. Struct. Biol.* **116,** 120–130.

Bartlett, N. M., Gillies, S. C., Bullivant, S., and Bellamy, A. R. (1974) Electron microscope study of reovirus reaction cores, *J. Virol.* **14,** 315–326.

Belnap, D. M., Olson, N. H., Cladel, N. M., Newcomb, W. W., Brown, J. C., Kreider, J. W., Christensen, N. D., and Baker, T. S. (1996) Conserved features in papilloma and polyoma virus capsids, *J. Mol. Biol.* **259,** 249–263.

Booy, F. P., Trus, B. L., Newcomb, W. W., Brown, J. C., Conway, J. F., and Steven, A. C. (1994) Finding a needle in a haystack: detection of a small protein (12-kDa VP26) in a large complex (the 200-MDa capsid of herpes simplex virus), *Proc. Natl. Acad. Sci. USA* **91,** 5652–5656.

Bottcher, B., Kiselev, N. A., Stel'mashchuk, V. Y., Perevozchikova, N. A., Borisov, A. V., and Crowther, R. A. (1997) Three-dimensional structure of infectious bursal disease virus determined by electron cryomicroscopy, *J. Virol.* **71,** 325–330.

Centonze, V. E., Chen, Y., Severson, T. F., Borisy, G. G., and Nibert, M. L. (1995) Visualization of single reovirus particles by low-temperature, high-resolution cryo-scanning electron microscopy, *J. Struct. Biol.* **115,** 215–225.

Cheng, R. H., Kuhn, R. J., Olson, N. H., Rossmann, M. G., Choi, H.-K., Smith, T. J., and Baker, T. S. (1995) Nucleocapsid and glycoprotein organization in an enveloped virus, *Cell* **80,** 621–630.

Cline, H. E., Lorensen, W. E., Ludke, S., Crawford, C. R., and Teeter, B. C. (1988) Two algorithms for the three-dimensional reconstruction of tomograms, *Med. Phys.* **15,** 320–327.

Conway, J. F., Trus, B. L., Booy, F. P., Newcomb, W. W., Brown, J. C., and Steven, A. C. (1996) Visualization of three-dimensional density maps reconstructed from cryoelectron micrographs of viral capsids, *J. Struct. Biol.* **116,** 200–208.

DeRosier, D. J. (1992) Whipping flagellin into shape, *Curr. Opin Struct. Biol.* **2,** 280–285.

Dryden, K. A., Wang, G., Yeager, M., Nibert, M. L., Coombs, K. M., Furlong, D. B., Fields, B. N., and Baker, T. S. (1993) Early steps in reovirus infection are associated with dramatic changes in supramolecular structure and protein conformation: analysis of virions and subviral particles by cryoelectron microscopy and image reconstruction, *J. Cell Biol.* **122,** 1023–1041.

Frank, J. (1997) The ribosome at higher resolution-the donut takes shape, *Curr. Opin. Struct. Biol.* **7,** 266–272.

Fuller, S. D. (1987) The T = 4 envelope of Sindbis virus is organized by interactions with a complementary T = 3 capsid, *Cell* **48,** 923–934.

Furlong, D. B., Nibert, M. L., and Fields, B. N. (1988) Sigma 1 protein of mammalian reoviruses extends from the surfaces of viral particles, *J. Virol.* **62,** 246–256.

Grant, R. A., Cranic, S., and Hogle, J. M. (1992) Radial depth provides the cue. *Curr. Biol.* **2,** 86–87.

Griffith, J. P., Griffith, D. L., Rayment, I., Murakami, W. T., and Caspar, D. L. D. (1992) Inside polyomavirus at 25-Å resolution, *Nature* **355,** 652–654.

Halse, M.-A. (1992) IRIS Explorer User's Guide. Silicon Graphics, Mountain View, CA.

Koonin, E. V. (1993) Computer-assisted identification of a putative methyltransferase domain in ns5 protein of flaviviruses and λ2 protein of reovirus, *J. Gen. Virol.* **74,** 733–740.

Kühlbrandt, W., Wang, D. N., and Fujiyoshi, Y. (1994) Atomic model of plant light-harvesting complex by electron crystallography, *Nature (London)* **367,** 614–621.

Lawton, J. A., Estes, M. K., and Prasad, B. V. V. (1997) Three-dimensional visualization of mRNA release from actively transcribing rotavirus particles, *Nature Struct. Biol.* **4,** 118–120.

Mao, Z. X., and Joklik, W. K. (1991) Isolation and enzymatic characterization of protein λ2, the reovirus guanylyltransferase, *Virology* **185,** 377–386.

Metcalf, P., Cyrklaff, M., and Adrian, M. (1991) The three-dimensional structure of reovirus obtained by cryo-electron microscopy, *EMBO J.* **10,** 3129–3136.

Morgan, D. G., Owen, C., Melanson, L. A., and DeRosier, D. J. (1995) Structure of bacterial flagellar filaments at 11 Å resolution: packing of the α-helices, *J. Mol. Biol.* **249,** 88–110.

Namba, K., Caspar, D. L. D., and Stubbs, G. (1988) Enhancement and simplification of macromolecular images, *Biophys. J.* **53,** 469–475.

Namba, K., Yamashita, I., and Vonderviszt, F. (1989) Structure of the core and central channel of bacterial flagella, *Nature (London)* **342,** 648–654.

Nibert, M. L., and Fields, B. N. (1992) A carboxy-terminal fragment of protein μ1/μ1C is present in infectious subvirion particles of mammalian reoviruses and is proposed to have a role in penetration, *J. Virol.* **66,** 6408–6418.

Nibert, M. L., and Fields, B. N. (1994) Early steps in reovirus infection of cells, *in* Wimmer, E. (Ed.), Cellular Receptors of Animal Viruses, pp. 341–364, Cold Spring Harbor Laboratory Press, Cold Spring Harbor, NY.

Nibert, M. L., Furlong, D. B., and Fields, B. N. (1991) Mechanisms of viral pathogenesis: Distinct forms of reoviruses and their

roles during replication in cells and host, *J. Clin. Invest.* **88,** 727–734.

Nibert, M. L., Schiff, L. A., and Fields, B. N. (1995) Reoviruses and their replication, *in* Fields, B. N., Knipe, D. M., and Howley, P. M. (Eds.), Fields Virology, 3rd ed., pp. 1557–1596, Lippincott-Raven Press, New York.

Olson, N. H., Kolatkar, P. R., Oliveira, M. A., Cheng, R. H., Greve, J. M., McClelland, A., Baker, T. S., and Rossmann, M. G. (1993) Structure of a human rhinovirus complexed with its receptor molecule, *Proc. Natl. Acad. Sci. USA* **90,** 507–511.

Powell, K. F., Harvey, J. D., and Bellamy, A. R. (1984) Reovirus RNA transcriptase: Evidence for a conformational change during activation of the core particle, *Virology* **137,** 1–8.

Prasad, B. V. V., Rothnagel, R., Zeng, C. Q.-Y., Jakana, J., Lawton, J. A., Chiu, W., and Estes, M. K. (1996) Visualization of ordered genomic RNA and localization of transcriptional complexes in rotavirus, *Nature* **382,** 471–473.

Prasad, B. V. V., Rothnagel, R., Jiang, X., and Estes, M. K. (1994) Three-dimensional structure of baculovirus-expressed Norwalk virus capsids, *J. Virol.* **68,** 5117–5125.

Radermacher, M., and Frank, J. (1984) Representation of three-dimensionally reconstructed objects in electron microscopy by surfaces of equal density, *J. Microsc.* **136,** 77–85.

Reed, L. J., and Hackert, M. L. (1990) Structure-function relationships in dihydrolipoamide acyl-transferases, *J. Biol. Chem.* **265,** 8971–8974.

Rossmann, M. G., Arnold, E., Erickson, J. W., Frankenberger, E. A., Griffith, J. P., Hecht, H. J., Johnson, J. E., Kamer, G., Luo, M., Mosser, A. G., Rueckert, R. R., Sherry, B., and Vriend, G. (1985) Structure of a human cold virus and functional relationship to other picornaviruses, *Nature* **317,** 145–153.

Rueckert, R. R. (1995) Picornaviridae and their replication, *in* Fields, B. N., Knipe, D. M., and Howley, P. M. (Eds.), Fields Virology, 3rd ed., pp. 609–654, Lippincott-Raven Press, New York.

Salunke, D. M., Caspar, D. L. D., and Garcea, R. L. (1989) Polymorphism in the assembly of polyomavirus capsid protein VP_1, *Biophys. J.* **56,** 887–900.

Schrag, J. D., Prasad, B. V. V., Rixon, F. J., and Chiu, W. (1989) Three-dimensional structure of the HSV1 nucleocapsid, *Cell* **56,** 651–660.

Sgro, J.-Y. (1996) Virus visualization, *in* Webster, R. G., and Granoff, A. (Eds.), Encyclopedia of Virology Plus (CD-ROM version), Academic Press, San Diego, CA.

Sherry, B., Mosser, A. G., Colonno, R. J., and Rueckert, R. R. (1986) Use of monoclonal antibodies to identify four neutralization immunogens on a common cold picornavirus, human rhinovirus 14, *J. Virol.* **57,** 246–257.

Speir, J. A., Munshi, S., Wang, G., Baker, T. S., Baker, T. S., and Johnson, J. E. (1995) Structures of the native and swollen forms of cowpea chlorotic mottle virus determined by X-ray crystallography and cryo-electron microscopy, *Structure* **3,** 63–78.

Stark, H., Mueller, F., Orlova, E. V., Schatz, M., Dube, P., Erdemir, T., Zemlin, F., Brimacombe, R., and van Heel, M. (1995) The 70S *Escherichia coli* ribosome at 23 Å resolution: fitting the ribosomal RNA, *Structure* **3,** 815–821.

Starnes, M. C., and Joklik, W. K. (1993) Reovirus protein λ3 is a poly(C)-dependent poly(G) polymerase, *Virology* **193,** 356–366.

Stoops, J. K., Baker, T. S., Schroeter, J. P., Kolodziej, S. J., Niu, X.-D., and Reed, L. J. (1992) Three-dimensional structure of the truncated core of the *Saccharomyces cerevisiae* pyruvate dehydrogenase complex determined from negative stain and cryoelectron microscopy images, *J. Biol. Chem.* **267,** 24769–24775.

Thurman-Commike, P. A., Greene, B., Jakana, J., Prasad, B. V. V., King, J., Privelige, P. E., Jr., and Chiu, W. (1996) Three-dimensional structure of scaffold-containing phage P22 procapsids by electron cryo-microscopy, *J. Mol. Biol.* **260,** 85–98.

Trachtenberg, S., and DeRosier, D. J. (1991) A molecular switch: subunit rotations involved in the right-handed to left-handed transitions in *Salmonella typhimurium* flagellar filaments, *J. Mol. Biol.* **220,** 67–77.

Trus, B. L., Roden, R. B. S., Greenstone, H. L., Vrhel, M., Schiller, J. T., and Booy, F. P. (1997) Novel structural features of bovine papillomavirus capsid revealed by a three-dimensional reconstruction to 9 Å resolution, *Nature Struct. Biol.* **4,** 413–420.

van Heel, M. (1983) Stereographic representation of three-dimensional density distributions, *Ultramicroscopy* **11,** 307–314.

Xu, P., Miller, S. E., and Joklik, W. K. (1993) Generation of reovirus core-like particles in cells infected with hybrid vaccinia viruses that express genome segments L1, L2, L3, and S2, *Virology* **197,** 726–731.

Yeager, M., Berriman, J. A., Baker, T. S., and Bellamy, A. R. (1994) Three-dimensional structure of the rotavirus haemagglutinin VP4 by cryo-electron microscopy and difference map analysis, *EMBO J.* **13,** 1011–1018.

Yeager, M., Weiner, S., and Coombs, K. M. (1996) Transcriptionally active reovirus core particles visualized by electron cryomicroscopy and image reconstruction, *Biophys. J.* **70,** A116.

Zhou, Z. H., Prasad, B. V. V., Jakana, J., Rixon, F. J., and Chiu, W. (1994) Protein subunit structure in herpes simplex virus A-capsid determined from 400 kV spot-scan electron cryomicroscopy, *J. Mol. Biol.* **242,** 456–469.